Water Supply

Water Supply Vol 22 No 1, 409 doi: 10.2166/ws.2021.260

Activated carbon incorporation on forward osmosis membrane surface for enhanced performance

Reshma Lakra[a], Malini Balakrishnan[b] and Subhankar Basu[a,*]

[a] Department of Applied Sciences and Humanities, National Institute of Foundry and Forge Technology (NIFFT), Ranchi, Jharkhand 834003, India
[b] The Energy and Resources Institute (TERI), Darbari Seth Block, IHC Complex, Lodhi Road, New Delhi 110003, India
*Corresponding author. E-mails: basusubhankar4@gmail.com; Subhankar.nifft@gov.in

ABSTRACT

Cellulose triacetate (CTA) is the first-generation forward osmosis (FO) membrane used for desalination. There have been a few chemical modifications of the CTA membrane surface. This has improved membrane hydrophilicity, water flux, and salt rejection compared with unmodified CTA membranes. Chitosan-containing porous materials as composites have resulted in increased pore characteristics. It has motivated the modification of the surface of the commercial CTA forward osmosis (FO) membrane by surface coating with chitosan (CS)–powdered activated carbon (AC) mix. The membrane morphology was characterized by SEM, FTIR-ATR, contact angle measurement and AFM. Operational conditions for FO such as the orientation of the membrane active layer, feed and draw solution flow rates, and type and concentration of draw salt were optimized with the original CTA membrane. The modified membrane exhibited around a two-fold increase in the water flux and reduced reverse salt flux compared with the original CTA membrane. The improved water flux was attributed to the CS-AC coating enhancing water wettability of the membrane surface and the porous AC generating additional water flow channels. Overall, the water flux of the CTA-CS-AC membrane developed in this work was superior to that of CTA and cellulose acetate (CA) membranes reported in the literature.

Key words: activated carbon-chitosan mix, desalination, forward osmosis, hydrophilic, surface modification

HIGHLIGHTS

- Incorporation of porous materials on membrane surface.
- Enhanced water flux.
- High salt rejection.
- Better performance than commercial and literature-reported membranes.
- Improved desalination process.

GRAPHICAL ABSTRACT

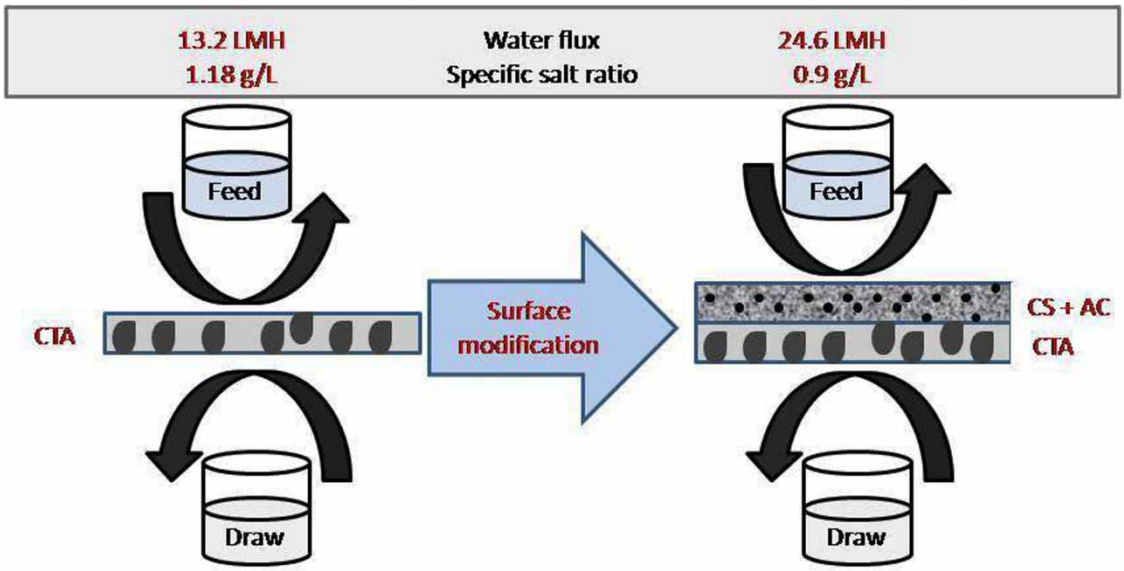

INTRODUCTION

To address the diminishing supply of quality freshwater in water-scarce regions, impaired sources such as seawater, brackish water and various wastewaters are being exploited for freshwater recovery (Tang *et al.* 2009; Sun *et al.* 2014). Among the technologies employed, membrane separation is a promising option to address the water crisis in the 21st century (Sun *et al.* 2014). In particular, the high-pressure-driven reverse osmosis (RO) process has been extensively employed for both large-scale desalination of brackish water and seawater as well as for the tertiary treatment of municipal wastewater (Kornboonraksa 2016). Though well-established, RO is beset by high cost resulting from being energy-intensive; in addition, its membrane fouling propensity requires periodic, costly membrane replacement (Liyanaarachchi *et al.* 2014; Motsa *et al.* 2014).

As an alternative to RO, forward osmosis (FO) has gained much attention for various applications in recent years. In RO, the driving force is the applied pressure difference, while in FO the process is driven by the osmotic pressure difference between a concentrated draw solution and a diluted feed solution across the semi-permeable membrane (Akther *et al.* 2015; Wang *et al.* 2018). Compared with RO, FO has very high water-recovery, low membrane-fouling tendency and greater energy efficiency (Zamani *et al.* 2015; Ang *et al.* 2019). These advantages of FO have attracted the attention of both academic researchers and industries (Shaffer *et al.* 2015). Besides desalination, FO applications have been reported in various fields such as food processing, domestic and industrial wastewater treatment, and power generation (Wang *et al.* 2018; Singh *et al.* 2019a, 2019b).

Despite the promise shown by FO, there are several challenges that need to be overcome for successful implementation of this technology. These include high reverse salt flux, internal and external concentration polarization leading to low water flux and high energy requirement for the regeneration and recovery of water from draw solution (Lutchmiah *et al.* 2014). All these aspects are interdependent. In recent reviews, the following aspects have been suggested for future research on FO: (i) preparation of new FO membranes with new materials or modification of existing FO membrane for improved performance, (ii) development of new integrated and hybrid FO processes for various applications including desalination, (iii) study of membrane-fouling phenomena and cleaning operations, (iv) mathematical modelling and simulation to understand the factors that influence FO performance, and (v) study of different types of draw solutes and their easy regeneration (Ang *et al.* 2019; Suwaileh *et al.* 2020).

FO membrane development has been grouped into three classes based on the material and their fabrication: (i) cellulose-based, (ii) thin-film composite (TFC), and (iii) chemically modified membranes (Saren *et al.*, 2011). Internal concentration polarization (ICP) and external concentration polarization (ECP) remain a challenge that can be addressed by improving the surface properties of the FO membrane. Generally, ICP (that decreases water flux and increases reverse salt flux) is closely

related to the thickness and porosity of the support layer (Gao *et al.* 2014). Chemical modification approaches especially of the top active surface layer can be a way to decrease ECP (Fu *et al.* 2021). The first-generation FO cellulose triacetate (CTA) membrane commercially available from Hydration Technology Inc. (HTI), USA, has been extensively studied for desalination. However, it is characterized by the drawbacks of relatively low water permeability, low salt rejection, and poor resistance to biochemical degradation (Suwaileh *et al.* 2020). Recent studies have reported an improvement in the properties of CTA membrane by incorporating porous materials e.g., carbon nanotubes (CNTs) (Choi *et al.* 2015), iron nanoparticles (Chi *et al.* 2017), graphene oxide (GO) (Li *et al.* 2017), and metal organic frameworks (Wang *et al.* 2019).

There are several studies on commercial RO and nanofiltration (NF) membranes coated with a variety of polymers to increase their active layer robustness and antifouling properties (Choudhury *et al.* 2018; Sharma *et al.* 2021). This is generally achieved by applying neutral or hydrophilic polymers to the existing membrane active layer thereby decreasing the surface roughness and minimizing the surface charge. The method of active layer modification of FO membranes employed by HTI is proprietary. Other similar studies on CTA FO membranes are limited, e.g., CTA FO membrane was modified via interfacial polymerization of *m*-phenylene diamine (MPD) trimesoyl chloride (TMC) (Wu *et al.* 2018). The study shows that a hydrophilic CTA porous membrane of thickness 102 $\pm$ 16 μm and porosity 87% improves the water flux and salt rejection. In another study, dip-coating with polyvinyl alcohol (PVA) resulted in a 20% increase in water flux compared with the unmodified membrane and without any salt leakage (Ahn *et al.* 2015). Commercial CTA membranes were modified by plasma-grafting polymerization, which resulted in the improvement of water flux and anti-protein-fouling properties of an FO membrane (Khongnakorn *et al.* 2020); gamma-ray irradiation of commercial CTA membrane improved membrane surface hydrophilicity, and it showed increased water flux and retention of Co and Sr (Liu *et al.* 2020). Coating of the membrane surface results in an additional layer to achieve the desired performance. Membrane surface coating enhances surface charge and hydrophilicity and decreases surface roughness (Miller *et al.* 2017). But, it also increases the membrane resistance to water flux (Liu *et al.* 2021). Thus, it is essential to look for a method that will not decrease the desirable properties of the membrane.

Table 1 shows that the addition of porous materials (activated carbon, biochar, carbon nanotubes, and graphene oxide) in CS improves the surface area, total pore volume and average pore size of the composite compared with CS (Hydari *et al.* 2012; Nitayaphat & Jintakosol 2015; Debnath *et al.* 2017; Khakpour & Tahermansouri 2018; Banu *et al.* 2019). Recently, tannic-acid–ferric (TA-Fe) complex coated on top of a commercial CTA-FO membrane purchased from Fluid Technology Solutions, Inc. (FTS) (Albany, OR, USA), showed enhanced water flux, improved antifouling property, and micropollutant removal (Liu *et al.* 2021). Similar improvement in membrane performance was reported with a polydopamine (PDA) coating on a commercial thin-film composite (TFC) FO membrane obtained from Hydration Technology Innovations (HTI) (Guo *et al.* 2018).

The present study aims to improve the properties of commercial CTA membrane by modifying its active surface using hydrophilic chitosan (CS), an organic biopolymer and porous powdered activated carbon (AC). CS, an abundant biomaterial obtained from crustacean seafood, is inexpensive, non-toxic, biodegradable, and environmentally friendly. Its molecular structure contains a good number of amino (-NH_2) and hydroxyl (-OH) functional groups which can enhance the wettability of AC (Shanmugam *et al.* 2016). Powdered AC is characterized by small particle size (<100 μm), and a high degree of microporosity and surface area (800–1,000 m^2/g). However, the behaviour of CS-AC coated CTA membrane is unknown.

In this study, commercial CTA membranes modified with CS-AC mix were prepared and characterized. Operation conditions for FO such as flow rate, membrane orientation, draw solution concentration and types of draw salts were initially

Table 1 | Pore characteristics of chitosan-containing materials

Materials	S_{BET} (m^2/g)	V_t (cm^3/g)	d_p (nm)	References
Chitosan	16.37	0.019	4.49	Hydari *et al.* (2012), Nitayaphat & Jintakosol (2015), Banu *et al.* (2019)
Chitosan-AC	147.85	0.227	7.32	
Chitosan-BC	34.34	0.052	3.21	
Chitosan	2.63	0.031	3.55	Khakpour & Tahermansouri (2018)
Chitosan-CNTs	104.00	1.220	14.30	
Chitosan	28.12	0.045		Debnath *et al.* (2017)
Chitosan-GO	37.37		13.67	

S_{BET}: BET surface area; V_t: total pore volume; d_p: average pore diameter; AC: activated carbon; BC: biochar; CNTs: carbon nanotubes; GO: graphene oxide.

optimized with the original CTA membrane and the modified membranes' performance tested under optimal conditions. The performance of the membranes developed in this work was also compared with reported literature on commercial CTA and cellulose acetate (CA) FO membranes.

MATERIALS AND METHODS

Chemicals and reagents

CTA FO membrane was purchased from Tech Inc. Incubating Technologies (Tech Inc.), Chennai, India. As per the supplier specifications, the 180–200 μm thick membrane was stable at pH 4–8, operating temperature of 20–50 °C and had a chlorine tolerance of 0.1 g/L. It was characterized by a pure water flux (J_w) of 15–20 L/m^2 h (with 2 M NaCl as draw solution) and reverse salt flux (J_s) of less than 0.20 g/m^2 h. The membranes were rinsed repeatedly with deionized (DI) water and stored at 4 °C before use. Chemicals and reagents were purchased from various local suppliers: Loba Chemie Pvt Ltd (NaCl, $MgCl_2 \cdot 6H_2O$); Merck Life Science Pvt Ltd (Na_2SO_4, H_2SO_4, glutaraldehyde 25% aqueous solution, glacial acetic acid, CS flakes from shrimp shells 75% deacetylated); Himedia Lab Pvt Ltd (powdered activated carbon); Merck Specialities Pvt Ltd ($MgSO_4 \cdot 7H_2O$). All chemicals were used as received without further purification.

Preparation of CTA-CS-AC FO membranes

The CS-AC mix was prepared at room temperature as follows. CS (1.0 g) was dissolved in glacial acetic acid (2 g) and DI water (100 mL) for 8 h. Then AC (0, 0.05, 0.1, 0.2 w/v %) was added in the CS solution and the mixture stirred using a magnetic stirrer (REMI 2ML, India) for one day. Thereafter, the solution was kept idle for another one day before being used for membrane modification. The CTA membrane was fixed in a rectangular wooden frame and the CS-AC mix was poured on top of it to coat the surface. The ensemble was kept horizontal for 3 min and then tilted to an angle of 60° to drain off the excess solution. The coated membrane was removed from the frame and kept for 1 h in the cross-linking solution (mixture of 25 mL of 25% glutaraldehyde solution, 0.11 g Na_2SO_4 and 0.2 mL conc. H_2SO_4, made-up to 250 mL with DI water). The modified membrane was then repeatedly washed five times to remove any unreacted CS. The membrane samples were kept soaked in water and tested on the same day. Figure 1 shows the schematic representation of the chemical reaction between CS and AC and the synthesis of the CS-AC mix.

FO operations

The schematic representation of the experimental set-up is shown in Figure 2. The FO laboratory-scale cross-flow filtration unit used in this study was purchased from Tech Inc., Chennai, India. This test cell had an effective filtration area of 0.016275 m^2 (0.105 m × 0.155 m). The experiments were performed at 20, 40, 60 LPH (L/h) flow rate of feed solution (FS) and draw solution (DS) pumped in a counter-current flow arrangement using two peristaltic pumps (Rivotek 50171, Mumbai, India). Flow rate was controlled by adjusting the valve settings and was measured using in-line rotameters (CVG Technocrafts, Mumbai, India) on both FS and DS sides. Two overhead stirrers (Remi RQ 5, Elektrotechnick Ltd, India, operated continuously at 400 rpm) in the feed and draw containers were used to ensure solution homogeneity. A digital balance (A&D Company Ltd FX 5000 GD, Delhi, India) connected to a digital logging system (WinCT software) was used on the feed

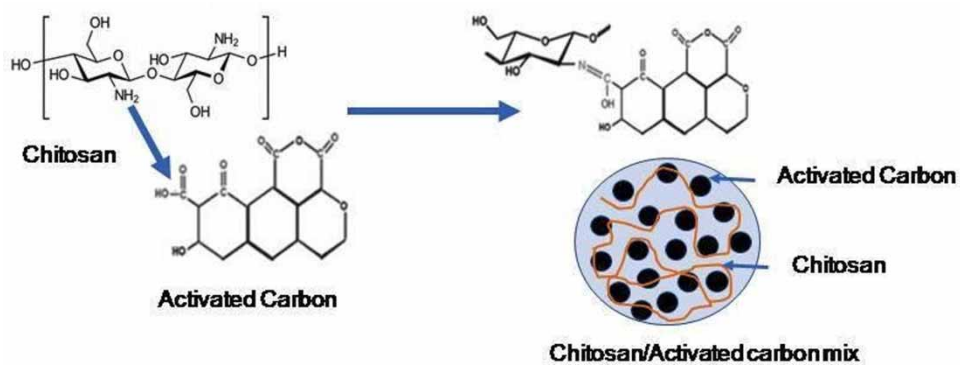

Figure 1 | The schematic representation of the synthesis of the CS-AC mix.

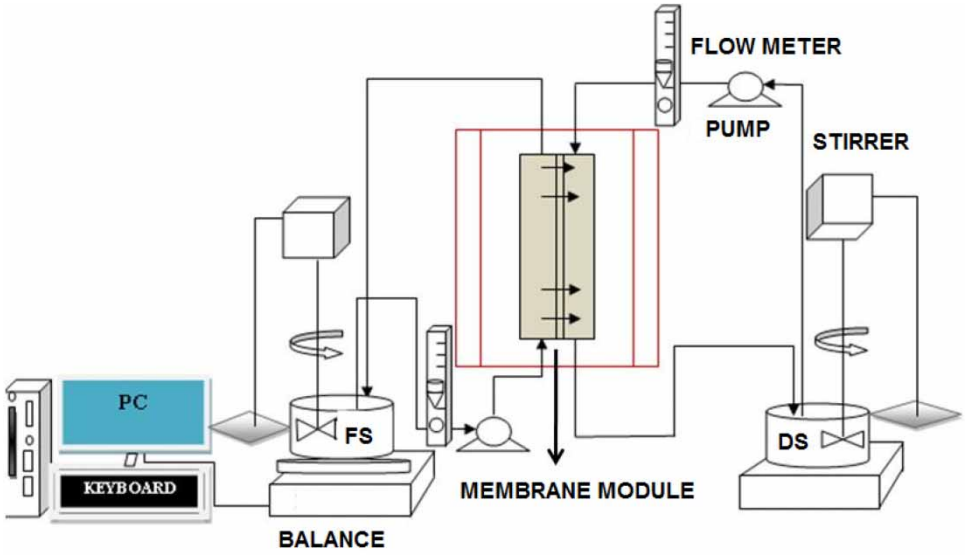

Figure 2 | Schematic diagram of the laboratory-scale FO experimental set-up.

side to monitor the change in the weight of the FS every 5 min. The change in weight of the FS was converted to water flux (J_w, L/m^2 h or LMH) using Equation (1):

$$J_w\ (\text{LMH}) = (W_i - W_t)/A \times \Delta t \tag{1}$$

where W_i is the initial weight (g) of the FS, W_t is the weight (g) of the FS at time t, A is the membrane cross-section area (m^2), and t is the filtration time (h). All experiments were conducted at an ambient temperature of 25 ± 2 °C. Change in the conductivity of the FS was recorded using a conductivity meter (Labindia, Mumbai, India). This data was used to calculate the reverse salt flux (J_s, g/m^2 h or GMH) as given in Equation (2):

$$J_s\ (\text{GMH}) = \frac{(C_t V_t - C_0 V_0)}{(A \times \Delta t)} \tag{2}$$

where V_0 and V_t are volume (L) of feed, C_0 and C_t are the salt concentration (mg/L) of FS; the subscripts 0 and t (h) are time at 0 and t.

From the J_w and J_s values obtained from Equations (1) and (2), the specific salt ratio was calculated by Equation (3):

$$\text{Specific salt ratio}\ (g/L) = J_s/J_w \tag{3}$$

Experimental methodology and performance analysis

The wet membrane was mounted in the FO cell and was initially flushed with DI water for an hour to ensure stable permeate flux. Then 1 L FS (DI water) and 1 L DS (NaCl, $MgCl_2{\cdot}6H_2O$, $MgSO_4{\cdot}7H_2O$ or Na_2SO_4) was circulated on the feed and draw sides, respectively. The draw salts were selected for high osmotic pressure ($MgCl_2$), moderate osmotic pressure (NaCl) and low osmotic pressure (Na_2SO_4, $MgSO_4$) (Yu *et al.* 2018). Each set of experiments, for optimizing a particular parameter, was done in triplicate and a fresh FO membrane was used for each set. Between the replicates, the membrane was cleaned by recirculating 0.5 L deionized water on both sides of the membrane for 30 min followed by flushing under tap water for 10 min. The water recovery (F_r) was calculated by Equation (4):

$$F_r\ (\%) = \frac{(\Delta V \times 100)}{V_0} \tag{4}$$

where ΔV is the difference in initial and final volume of FS, and V_0 is the initial volume.

The performance of the original CTA membrane was evaluated at different flow rates, active layer (AL) orientation, concentrations of DS and draw salts. The optimal operation conditions thus identified were then used to test the modified membrane samples. In all FO experiments, the water flux (J_w), reverse salt flux (J_s) and water recovery (F_r) was determined. The membranes were tested in FO mode (AL facing FS) and PRO mode (pressure retarded osmosis; AL facing DS). Water flux was measured in both the studies.

Membrane characterization

Fourier-transform infrared–attenuated total reflection (FTIR-ATR) spectroscopy (IR-Prestige 21, Shimadzu Corp., Japan) was used to analyze the membrane functional groups. Scanning electron microscopy (SEM, JSM-6390LV, Jeol, Japan) was used to investigate the morphologies of the membranes and AC. The membrane samples were prepared by freeze-fracturing under liquid nitrogen; both membrane and AC samples were coated with Au in an Ar atmosphere using a vacuum evaporator before SEM analysis. Atomic force microscopy (AFM, Solver Pro-47, NT-MDT, Russia) was used to evaluate the surface roughness of the membranes. The BET values and pore structure of AC was obtained from nitrogen adsorption isotherms at 77 K using a surface area analyzer (Quantachrome Instruments, USA). The water contact angle was measured by the sessile drop method using the set-up from Tech Inc., Chennai, India.

RESULTS AND DISCUSSION

Membrane characterization

Figure 3 shows the spectrum of the CTA (Figure 3(a)) and CTA-CS-AC (1% CS–0.2% AC) (Figure 3(b)) membranes. The amino and the hydroxyl groups are important functional groups of CS structure. The wide band detected in the 3,500–3,100 cm^{-1} region is ascribed to the O–H bond stretching modes. The peaks at 1,380 cm^{-1} indicate the –NH vibration in $–NH_2$. It also represents the interaction between the NH_2 groups in CS and OH groups of the CTA. The characteristic adsorption bands are located around 1,500 cm^{-1} and 1,755 cm^{-1}, due to stretching vibrations of the carbonyl group. The bands at 1,219 cm^{-1} and 1,055 cm^{-1} correspond to the stretching of C–O single bonds. The weak bands at 2,935 cm^{-1} and 2,888 cm^{-1} are attributed to C–H bonds. After modification of the membrane (Figure 3(b)), the carbonaceous content of AC shows intense bands between 3,200 cm^{-1} and 3,500 cm^{-1} (O–H and N–H stretching vibrations) (Amara *et al.* 2009; Queiroz *et al.* 2015; Shu *et al.* 2017). The peaks at 1,600 cm^{-1} and 1,420 cm^{-1} show stretching vibrations of C = O in the carbonyl group and deformation of C–O and O–H in carboxylic acid, respectively (Figure 1) (Nowruzi *et al.* 2020). The presence of the functional groups improves the membrane surface hydrophilicity, which eventually improves the membrane selectivity (Shakeri *et al.* 2017). The surface roughness of the membrane was studied by AFM (Figure 3(c) and 3(d)) and the roughness parameters calculated based on the AFM scanning area of 10 μm × 10 μm. The dark areas show the pores of the membrane, and the bright areas show the highest sites of the membrane surface. The R_a value of the CTA membrane is 15.45 nm, while the R_a value of the CTA-CS-AC (1% CS–0.2% AC) is 20.99 nm. The increased R_a value may result in improved water flux, followed by an increase in the area available for water transport (Hirose *et al.* 1996; Rana & Matsuura 2010). The SEM image of the CTA membrane surface (Figure 3(e)) shows a dense, smooth surface without any cracks. In the modified CTA-CS-AC (1% CS–0.2% AC) membrane (Figure 3(f)), the presence of powdered AC (Figure 3(g)) scattered on the surface is observed. The modified membrane surface seems to be non-uniform and irregular, as evident from the increased surface roughness value. It is interesting to note that the AC are completely wrapped in the CS matrix, and the AC are not visible in Figure 3(f), even at higher magnification, compared with Figure 3(g).

Performance of CTA membrane

The FO operational conditions were optimized with the original CTA membrane. Figure 4 shows the water flux and specific salt ratio of the original CTA membrane at different flow velocities (20 LPH, 40 LPH and 60 LPH) with 1M NaCl as DS. The active layer (AL) was facing the FS. Increasing the cross-flow rate from 20 LPH to 60 LPH results in marginal increase in water flux (from 8.27 LMH to 8.56 LMH) with a corresponding increase in the specific salt ratio (from 1.55 g/L to 1.70 g/L). This indicates that the water flux and specific salt ratio for this membrane are independent of the flow rate in the range tested, and there are no defects on the membrane separation layer. High flow velocities intensify the scouring on the membrane surface thereby lowering the chances of ECP, which is an undesirable phenomenon contributing to poor water flux (Qasim *et al.* 2015). Further, high flow rates of FS and DS enhance the mass transfer which, in turn, improves

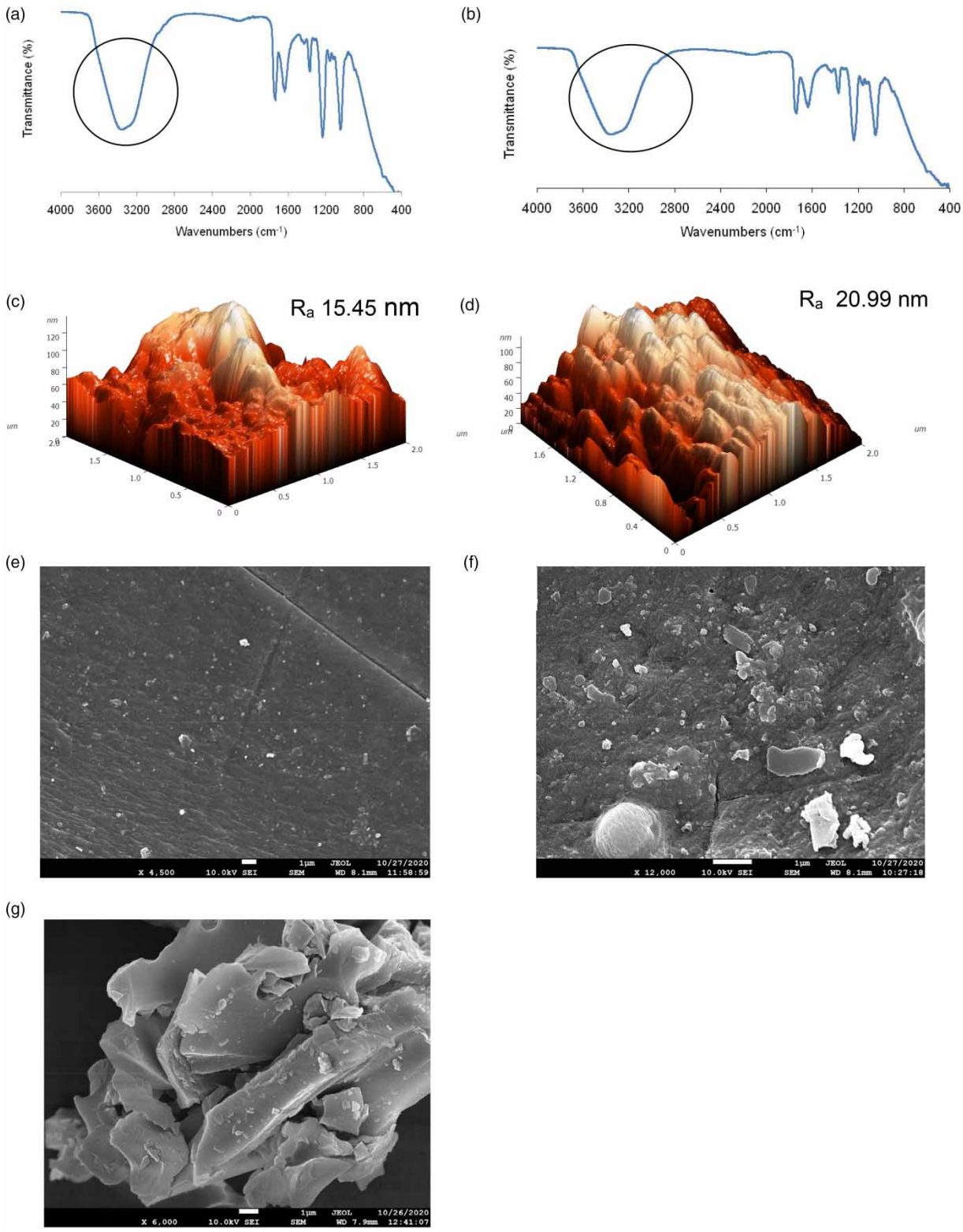

Figure 3 | Characterization of the FO membrane: (a) FTIR-ATR spectra of CTA, and (b) CTA-CS-AC (1% CS–0.2% AC) membrane; (c) AFM image of CTA membrane, (d) AFM image of CTA-CS-AC (1% CS–0.2% AC) membrane; SEM images of the surface of (e) CTA membrane (scale indicated by white bar), (f) CTA-CS-AC (1% CS–0.2% AC) membrane (scale indicated by white bar), and (g) powdered AC (scale indicated by white bar).

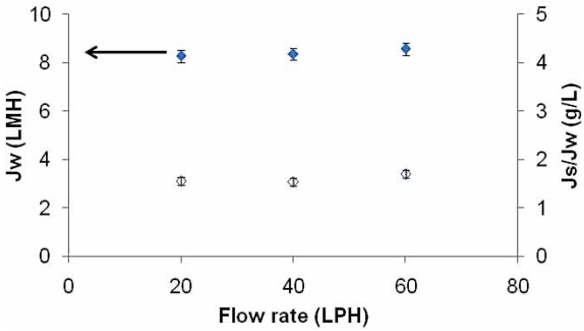

Figure 4 | CTA membrane performance at different cross-flow rates (FS: DI water, DS: 1M NaCl, active layer facing FS).

the permeate flux (Maouia *et al.* 2020). As higher cross-flow also leads to increased specific salt ratio, a flow rate of 40 LPH was chosen for further studies.

Table 2 shows a comparative study of the performance of commercial CTA membranes on changing the orientation of the membrane active layer (AL) towards FS (FO mode) and DS (PRO mode), respectively. The study shows that the water flux in PRO mode is more than in FO mode. It could be due to the internal concentration polarization (ICP). ICP occurs in a FO process when the water flows in the opposite direction to the solute flux. This can lead to either (i) a concentrative ICP, or (ii) a dilutive ICP. When the active layer is facing the draw solution (AL-DS), the solutes from the FS accumulate in the porous support layer due to their rejection by the active separation layer. This is called concentrative ICP. On the other hand, when the active layer is facing the feed solution (AL-FS), it results in dilution of the draw solution inside the support layer, and this is called dilutive ICP. However, in both cases, the effective osmotic pressure is reduced, decreasing the water flux (McCutcheon & Elimelech 2006; Tang *et al.* 2010). In PRO mode, the foulants deposited in the porous support result in membrane fouling and reduce the membrane cleaning efficiency (Qi *et al.* 2012). In the present study, in AL-FS (DI water) no ICP occurs. As it operates under low hydraulic pressure, no solute accumulates at the AL and the effect of ECP on the water flux is insignificant. Thus, all further FO experiments were conducted with AL oriented towards FS.

The effect of varying DS concentrations (0.5, 1.0, and 2.0 M NaCl) is shown in Figure 5. As the concentration of DS increases from 0.5 M to 2.0 M, the corresponding osmotic pressure of the DS increases from 24.6 atm to 98.4 atm. The increased differences in the pressure gradient across the membrane result in a rise in water flux from 4.33 LMH to 13.27 LMH, and a decrease in specific salt ratio from 1.8 to 1.18. The increase in water flux with an increasing osmotic pressure of the DS is reported in other works (Achilli *et al.* 2010; Liu *et al.* 2021). The specific salt ratio indicates the selectivity of the FO membrane. The decrease in specific salt ratio with increased DS concentration indicates low draw solute migration during the FO process and a highly efficient FO membrane (Fu *et al.* 2021).

In general, a DS with high osmotic pressure can generate high water flux (Achilli *et al.* 2010). Typically, selection of a suitable DS resulting in (i) high water flux, (ii) low reverse salt diffusion and (iii) easy recovery of the diluted DS is important for attaining high FO system performance (Chekli *et al.* 2012). Figure 6 shows the FO performance with different types of DS

Table 2 | Performance of commercial CTA membranes for desalination in FO and PRO mode of operations

Manufacturer	Draw solution (NaCl)	J_w (FO) (LMH)	J_w (PRO) (LMH)	References
Hydration Technology Innovations (HTI), USA	0.5 M	5	5.5	Manickam & McCutcheon (2015)
	1 M	6	11	
	1.5 M	8	14	
Fluid Technology Solutions Inc.(FTS), USA	0.5 M	8	12	Liu *et al.* (2021)
	1 M	10	20	
	1.5 M	12	21	
	2 M	14	22.5	
Tech Inc. India	0.5 M	4.33	6.21	Present study
	1 M	8.35	15.25	
	2 M	13.27	18.71	

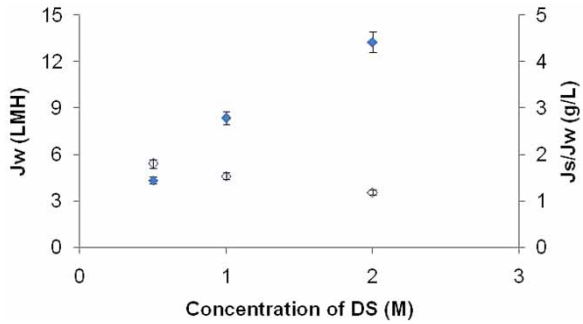

Figure 5 | CTA membrane performance at different NaCl DS concentrations (FS: DI water, cross-flow rate: 40 LPH).

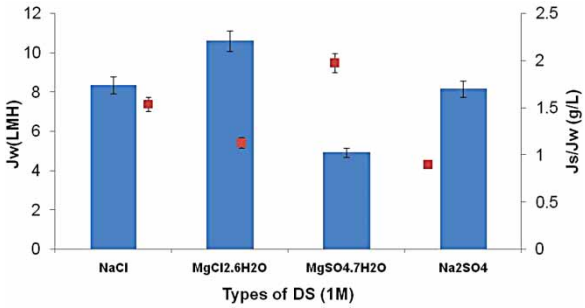

Figure 6 | CTA membrane performance with different draw solutions (FS: DI water, DS concentration: 1M, cross-flow rate: 40 LPH).

having different osmotic pressure at 1M concentration: NaCl: 47.5 atm, $MgCl_2{\cdot}6H_2O$: 150 atm, Na_2SO_4: 47 atm and $MgSO_4{\cdot}7H_2O$: 25 atm. The water flux for different DS follows the same order as the osmotic pressure with $MgCl_2{\cdot}6H_2O >$ NaCl, $Na_2SO_4 >$ $MgSO_4{\cdot}7H_2O$. The higher osmotic pressure of $MgCl_2{\cdot}6H_2O$ translates into a higher concentration gradient across the membrane; this results in higher water flux. The specific salt ratio of $MgCl_2{\cdot}6H_2O$ (1.132) is also lower than that of NaCl (1.537). The difference in water flux with different DS is due to ICP effects that reduce the effective osmotic pressure difference across the membrane (Achilli *et al.* 2010). The variation could also be due to the variation in the hydrated diameter of the anion (Cl^-: 300×10^{-12} m, SO_4^{2-}: 400×10^{-12} m) and cation (Mg^{+2}: 300×10^{-12} m, Na^+: 450×10^{-12} m) and its interaction with the negatively charged CTA membrane (Achilli *et al.* 2010; Phillip *et al.* 2010). In a similar attempt to identify suitable DS for desalination, different water flux and salt flux were reported for different salts at the same osmotic pressure but at different DS concentrations (Achilli *et al.* 2010). Although $MgCl_2{\cdot}6H_2O$ outperforms the other DS in this study, the next best option of NaCl was chosen for further experiments because it is cheaper (9 $/kg) than $MgCl_2{\cdot}6H_2O$ (26 $/kg) (using a conversion of 1$ = 73.51 INR).

Performance of CTA-CS-AC membranes

The properties of the powdered AC used in modifying the CTA membrane surface are summarized in Table 3.

In this work, the active layer of the commercial CTA membrane was modified with CS containing different concentrations of powdered AC. A positron annihilation lifetime spectroscopy (PALS) study shows that the active layer of CTA membranes is composed of uniform pores of size 0.29–0.30 nm (Kim *et al.* 2017). Further, Table 1 shows that the pore diameter of CS-AC increases to 7.32 nm. Thus, the addition of AC increases the size of the flow channels of the separation layers. In a separate study, we found that coating the CTA membrane with 1% CS produces higher water flux than coating with 0.5% or 2% CS (Supplementary Information, Table S1). Figure 7 shows the effect of varying AC loading on the performance of CTA-CS-AC membrane. The membrane with 0.1% AC loading (M-IV) displayed maximum water flux of 24.6 LMH compared with 13.2 LMH for the original membrane. Correspondingly the specific salt ratio decreased with AC loading, from 1.05 (original membrane) to 0.9 (0.1% AC). Surface modification decreased the membrane contact angle (Table 4) and improved the water wettability. The contact angle decrease was significant from 73.9° (original membrane) to around 10° (M-IV and M-V

Table 3 | Properties of powdered AC

Apparent density	Pore volume	BET surface area	Langmuir surface area	Average pore diameter (4 V/A by BET)
1,032 g/L	0.57 cm^3/g	990 m^2/g	1,183 m^2/g	2.37 nm

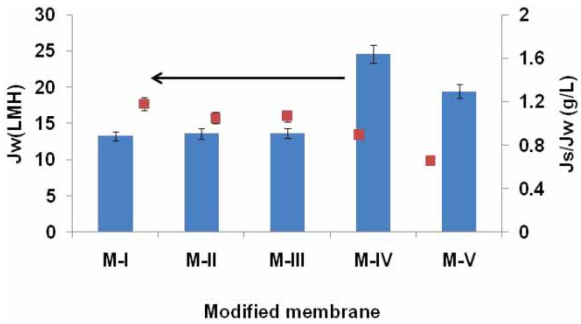

Figure 7 | Performance of CTA-CS-AC membranes with varying AC load (FS: DI water, DS: 2M NaCl, cross-flow rate: 40 LPH).

Table 4 | Contact angle of CTA-CS-AC membranes

Membrane	Details	Contact angle (°)
M-I	CTA	73.91
M-II	CTA-1%CS	33.0
M-III	CTA-1%CS-0.05%AC	32.0
M-IV	CTA-1%CS-0.1%AC	10.3
M-V	CTA-1%CS-0.2%AC	10.1

membranes with 0.1% and 0.2% AC loading respectively). Further, the high surface area and the well-defined porous structure of AC (Table 3) creates new water channels within the membrane surface resulting in higher water flux. The pore diameter of 2.37 nm readily allows passage of water molecules of diameter 0.275 nm while restricting salt migration from DS to FS. This observation is also supported by the increased R_a value of the CTA-CS-AC (0.2%) membrane (Figure 3(c)). However, there is a decrease in water flux with increased AC content (0.2%), possibly due to the formation of a denser CS-AC matrix.

Figure 8 displays the water recovery for the various membranes. The water recovery of the original CTA membrane was 30%, which increased marginally to 33% upon surface modification with CS. Incorporation of AC in CS resulted in further increase in water recovery up to 78% (M-IV with 0.1% AC loading). The increase in water recovery of over two-fold is due to

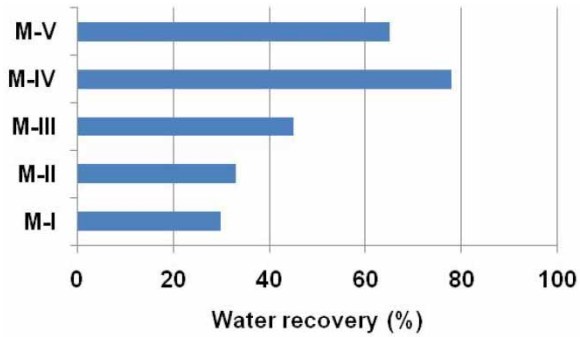

Figure 8 | The water recovery (%) of CTA, CTA-CS and CTA-CS-AC membranes (FS: DI water, DS: 2M NaCl, cross-flow rate: 40 LPH).

the increased hydrophilicity and the presence of porous AC which generates well-defined water channels within the membrane surface layer, resulting in high water flux and reduced ECP. Secondly, the hydrophilic properties are desirable in FO membranes as they allow water molecules to readily pass through the internal fine pores of the membranes, improving overall performance. The hydrophilic CS polymer matrix has good compatibility with the AC. Finally, the increased surface roughness provides a higher filtration area for water transportation. These characteristics are expected to result in high stability of the coating during long-term operations.

Unlike this work that targeted the addition of a porous material layer on top of the CTA membrane surface, other literature studies involve the inclusion of porous materials in the CTA-FO membrane matrix itself. Particle content in the polymer matrix reportedly enhanced the water flux while reducing the specific salt ratio and ICP. For example, boehmite particles added to a cellulose acetate/cellulose triacetate mixture augmented the water flux three-fold (up to 21 LMH) (Zirehpour *et al.* 2015). Inclusion of acid-functionalized CNTs in cellulose acetate resulted in a 1.5 times increase in water flux (up to 14 LMH) (Choi *et al.* 2015). Metal organic framework (MIL-53) in cellulose acetate enhanced water flux 1.3 times (up to 34.9 LMH) (Wang *et al.* 2019). The results are comparable to that obtained in the present study with a water flux enhancement of 1.85 times (up to 24.6 LMH) with activated carbon incorporation on the CTA membrane surface. The present membrane showed better performance than polyvinyl alcohol/polydopamine-coated zeolitic imidazolate framework (PVA/PDA@ZIF-8)-coated polyether sulfone (PES) substrate (J_w 13 LMH) FO (Fu *et al.* 2021). Furthermore, the dip-coating procedure to modify the membrane surface used in this work is simple and replicable with other FO membranes; it can also be easily reproduced in the membrane manufacturing process. Wu *et al.* (2018) reported that increased CTA membrane thickness on coating with MPD-TMC solution affects the performance of the membrane. The study reported that the decreased membrane thickness (198 to 98 μm) improved the water flux by two times in FO and PRO mode. The best result was obtained with a thickness of 98 $\pm$ 15 μm. Figure 9 shows the SEM image of the modified membrane. The membrane shows an asymmetric structure with a support layer and a separation layer. The total thickness of the modified membrane was 90 $\pm$ 3 μm. Thus, appropriate membrane thickness and the improved surface properties (Table 1), with porous AC, resulted in the high water flux of the modified membranes.

Figure 10 shows the benefit of surface modification of the commercial FO membrane to reduce the effect of ICP. The modified membrane (M-IV) water flux and the three commercial CTA membranes were studied for both FO and PRO modes. The increased ratio of water flux (FO/PRO) of M-IV (94.6%) in comparison with the commercial CTA membranes (52% $\pm$ 2%) indicates that the modified membrane has a low degree of ICP (Li *et al.* 2016; Wang *et al.* 2016).

Table 5 presents a compilation of CA and CTA membranes tested for desalination. The comparison shows that the surface modification of the commercial CTA membrane by incorporating porous AC largely enhances the water flux compared with

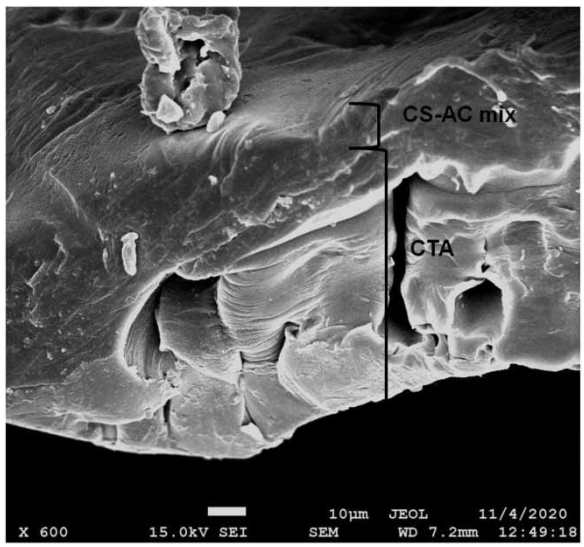

Figure 9 | SEM image of the cross-section view of commercial CTA membrane (scale indicated by white bar).

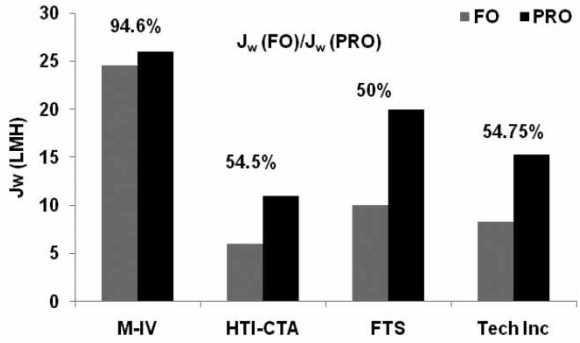

Figure 10 | A comparative study of the water flux under FO mode and PRO mode: HTI-CTA membrane, FTS membrane, Tech Inc. membrane, and present study (M-IV) membrane.

Table 5 | Comparison of FO membrane performance: this work and relevant literature reports

FO-Material	J_w (LMH)	J_s/J_w (g/L)	FS	DS	References
CA	10.3	0.0776	DI water	2M $MgCl_2$	Zhang *et al.* (2010)
CA	9.8	0.122	DI water	2M $MgCl_2$	Zhang *et al.* (2010)
CA	7.4		DI water	2M NaCl	Ahn *et al.* (2015)
CA	10	0.396	DI water	2M NaCl	Zhang *et al.* (2011)
CA	1.3		35 g/L NaCl	150 g/L $MgSO_4$	Sairam *et al.* (2011)
Modified CA	6.8		35 g/L NaCl	150 g/L $MgSO_4$	
CTA	13.7	0.005	DI water	2M NaCl	Heo *et al.* (2016)
CTA	2.6	0.47	DI water	1M $Al_2(SO_4)_3$	Maouia *et al.* (2020)
CTA	6.0	0.2	DI water	0.5M NaCl	Xiao *et al.* (2017)
CTA	6.9		0.1M NaCl	2M glucose	Chen *et al.* (2017)
CTA	5		10 mM NaCl	0.5M NaCl	Wei *et al.* (2011)
CTA	7.5	0.167	DI water	1M NaCl	Ren & McCutcheon (2014)
CTA	3.4		0.5M NaCl	2M glucose	Li *et al.* (2016)
CTA	7.5		0.5M NaCl	2M glucose	Li *et al.* (2013)
CTA	3.7	0.43	Brackish water	0.7M $FeSO_4$	Qasim *et al.* (2017)
	1.6		Seawater	0.7M $FeSO_4$	
CA-PVA coating	8.8		DI water	1.5M NaCl	Ahn *et al.* (2015)
CTA-MPD-TMC coating	11.7	0.587	DI water	0.5M NaCl	Wu *et al.* (2018)
CTA	13.2	1.18	DI water	2M NaCl	Present work
CTA-1%CS	13.6	1.02	DI water	2M NaCl	
CTA-1%CS-0.05%AC	13.6	0.98	DI water	2M NaCl	
CTA-1%CS-0.1%AC	24.6	0.9	DI water	2M NaCl	
CTA-1%CS-0.2%AC	19.4	0.665	DI water	2M NaCl	

the original membrane. The membranes prepared in the present work, especially M-IV (CTA-1%CS-0.1%AC), are particularly promising.

CONCLUSIONS

Under the conditions of this study, the following optimal conditions for FO with commercial CTA membranes were identified: (i) membrane active layer oriented towards feed solution; (ii) feed and draw solution flow rate of 40 LPH; and

(iii) draw of NaCl at 2M concentration. The performance, in terms of higher water flux and lower specific salt ratio, can be improved by membrane surface modification. This was successfully accomplished by coating the CTA membrane with a mix of chitosan and powdered activated carbon. CTA coated with 1% chitosan loaded with 0.1% activated carbon exhibited the best performance. Surface modification of the membrane surface with a porous coating is thus a simple and promising approach to improve FO membrane performance.

ACKNOWLEDGEMENTS

The authors wish to acknowledge Science & Engineering Research Board (SERB), Department of Science and Technology, Government of India, for their financial support (File No. CRG/2018/003463).

CONFLICT OF INTEREST

The authors Reshma Lakra, Malini Balakrishnan, and Subhankar Basu certify that there is no conflict of interest in the paper entitled 'Activated Carbon Incorporation on Forward Osmosis Membrane Surface for Enhanced Performance'.

DATA AVAILABILITY STATEMENT

All relevant data are included in the paper or its Supplementary Information.

REFERENCES

Achilli, A., Cath, T. Y. & Childress, A. E. 2010 Selection of inorganic-based draw solutions for forward osmosis applications. *J. Membr. Sci.* **364**, 233–241.

Ahn, H. R., Tak, T. M. & Kwon, Y.-N. 2015 Preparation and applications of poly vinyl alcohol (PVA) modified cellulose acetate (CA) membranes for forward osmosis (FO) processes. *Desalin. Water Treat.* **53**, 1–7.

Akther, N., Sodiq, A., Giwa, A., Daer, S., Arafat, H. A. & Hasan, S. W. 2015 Recent advancements in forward osmosis desalination: a review. *Chem. Eng. J.* **281**, 502–522.

Amara, M., Arous, O., Smail, F., Kerdjoudj, H., Trari, M. & Bouguelia, A. 2009 An assembled poly-4-vinyl pyridine and cellulose triacetate membrane and Bi_2S_3 electrode for photoelectrochemical diffusion of metallic ions. *J. Hazard. Mater.* **169**, 195–202.

Ang, W. L., Mohammad, A. W., Johnson, D. & Hilal, N. 2019 Forward osmosis research trends in desalination and wastewater treatment: a review of research trends over the past decade. *J. Water Process Eng.* **31**, 100886.

Banu, H. T., Karthikeyan, P. & Meenakshi, S. 2019 Zr^{4+} ions embedded chitosan-soya bean husk activated bio-char composite beads for the recovery of nitrate and phosphate ions from aqueous solution. *Int. J. Biol. Macromol.* **130**, 573–583.

Chekli, L., Phuntsho, S., Shon, H. K., Vigneswaran, S., Kandasamy, J. & Chanan, A. 2012 A review of draw solutes in forward osmosis process and their use in modern applications. *Desalin. Water Treat.* **43**, 167–184.

Chen, X., Xu, J., Lu, J., Shan, B. & Gao, C. 2017 Enhanced performance of cellulose triacetate membranes using binary mixed additives for forward osmosis desalination. *Desalination* **405**, 68–75.

Chi, X. Y., Zhang, P. Y., Guo, X. J. & Xu, Z. L. 2017 Interforce initiated by magnetic nanoparticles for reducing internal concentration polarization in CTA forward osmosis membrane. *J. Appl. Polym. Sci.* **134**, 44852.

Choi, H., Son, M., Yoon, S. H., Celik, E., Kang, S., Park, H., Park, C. H. & Choi, H. 2015 Alginate fouling reduction of functionalized carbon nanotube blended cellulose acetate membrane in forward osmosis. *Chemosphere* **136**, 204–210.

Choudhury, R. R., Gohil, J. M., Mohanty, S. & Nayak, S. K. 2018 Antifouling, fouling release and antimicrobial materials for surface modification of reverse osmosis and nanofiltration membranes. *J. Mater. Chem. A* **6**, 313–333.

Debnath, S., Parashar, K. & Pillay, K. 2017 Ultrasound assisted adsorptive removal of hazardous dye Safranin O from aqueous solution using crosslinked graphene oxide–chitosan (GO–CH) composite and optimization by response surface methodology (RSM) approach. *Carbohydr. Polym.* **175**, 509–517.

Fu, W., Chen, J., Li, C., Jiang, L., Qiu, M., Li, X., Wang, Y. & Cui, L. 2021 Enhanced flux and fouling resistance forward osmosis membrane based on a hydrogel/MOF hybrid selective layer. *J. Colloid Interface Sci.* **585**, 158–166.

Gao, Y., Wang, Y., Li, W. & Tang, C. Y. 2014 Characterization of internal and external concentration polarizations during forward osmosis processes. *Desalination* **338**, 65–73.

Guo, H., Yao, Z., Wang, J., Yang, Z., Ma, X. & Tang, C. Y. 2018 Polydopamine coating on a thin film composite forward osmosis membrane for enhanced mass transport and antifouling performance. *J. Membr. Sci.* **551**, 234–242.

Heo, J., Chu, K. H., Her, N., Im, J., Park, Y. G., Cho, J., Sarp, S., Jang, A., Jang, M. & Yoon, Y. 2016 Organic fouling and reverse solute selectivity in forward osmosis: role of working temperature and inorganic draw solutions. *Desalination* **389**, 162–170.

Hirose, M., Ito, H. & Kamiyama, Y. 1996 Effect of skin layer surface structures on the flux behaviour of RO membranes. *J. Membr. Sci.* **121**, 209–215.

Hydari, S., Sharififard, H., Nabavinia, M. & Parvizi, M. R. 2012 A comparative investigation on removal performances of commercial activated carbon, chitosan biosorbent and chitosan/activated carbon composite for cadmium. *Chem. Eng. J.* **193–194**, 276–282.
Khakpour, R. & Tahermansouri, H. 2018 Synthesis, characterization and study of sorption parameters of multi-walled carbon nanotubes/chitosan nanocomposite for the removal of picric acid from aqueous solutions. *Int. J. Biol. Macromol.* **109**, 598–610.
Khongnakorn, W., Bootluck, W. & Jutaporn, P. 2020 Surface modification of FO membrane by plasma-grafting polymerization to minimize protein fouling. *J. Water Process Eng.* **38**, 101633.
Kim, S. J., Kook, S., O'Rourke, B. E., Lee, J., Hwang, M., Kobayashi, Y., Suzuki, R. & Kim, I. S. 2017 Characterization of pore size distribution (PSD) in cellulose triacetate (CTA) and polyamide (PA) thin active layers by positron annihilation lifetime spectroscopy (PALS) and fractional rejection (FR) method. *J. Membr. Sci.* **527**, 143–151.
Kornboonraksa, T. 2016 Using tertiary-treated municipal wastewater as makeup water by reverse osmosis membrane. *Desalin. Water Treat.* **57**, 7422–7431.
Li, G., Li, X. M., He, T., Jiang, B. & Gao, C. 2013 Cellulose triacetate forward osmosis membranes: preparation and characterization. *Desalin. Water Treat.* **51**, 2656–2665.
Li, G., Wang, J., Hou, D., Bai, Y. & Liu, H. 2016 Fabrication and performance of PET mesh enhanced cellulose acetate membranes for forward osmosis. *J. Environ. Sci.* **45**, 7–17.
Li, F., Sun, M., Cheng, Q., Tian, Q., Ma, C. & Huang, M. 2017 Characterization, and antifouling performance of cellulose triacetate forward osmosis membranes modified with graphene oxide. *Desal. Water Treat.* **62**, 31–42.
Liu, X., Wu, J., Hou, L. & Wang, J. 2020 Performance and deterioration of forward osmosis membrane exposed to various dose of gamma-ray irradiation. *Ann. Nucl. Energy* **135**, 106950.
Liu, S., Tong, X., Liu, S., An, D., Yan, J., Chen, Y. & Crittenden, J. 2021 Multi-functional tannic acid (TA)–ferric complex coating for forward osmosis membrane with enhanced micropollutant removal and antifouling property. *J. Membr. Sci.* **626**, 119171.
Liyanaarachchi, S., Shu, L., Muthukumaran, S., Jegatheesan, V. & Baskaran, K. 2014 Problems in seawater industrial desalination processes and potential sustainable solutions: a review. *Rev. Environ. Sci. Biotechnol.* **13**, 203–214.
Lutchmiah, K., Verliefde, A. R. D., Roest, K., Rietveld, L. C. & Cornelissen, E. R. 2014 Forward osmosis for application in wastewater treatment: a review. *Water Res.* **58**, 179–197.
Manickam, S. S. & McCutcheon, J. R. 2015 Model thin film composite membranes for forward osmosis: demonstrating the inaccuracy of existing structural parameter models. *J. Membr. Sci.* **483**, 70–74.
Maouia, D. B., Boubakri, A., Hafiane, A. & Bouguecha, S. 2020 Aluminum sulfate as an innovative draw solute for forward osmosis desalination. *Chem. Africa* **3**, 141–152.
McCutcheon, J. R. & Elimelech, M. 2006 Influence of concentrative and dilutive internal concentration polarization on flux behavior in forward osmosis. *J. Membr. Sci.* **284**, 237–247.
Miller, D. J., Dreyer, D. R., Bielawski, C. W., Paul, D. R. & Freeman, B. D. 2017 Surface modification of water purification membranes. *Angew. Chem.* **56**, 4662–4711.
Motsa, M. M., Mamba, B. B., D'Haese, A., Hoek, E. M. V. & Verliefde, A. R. D. 2014 Organic fouling in forward osmosis membranes: the role of feed solution chemistry and membrane structural properties. *J. Membr. Sci.* **460**, 99–109.
Nitayaphat, W. & Jintakosol, T. 2015 Removal of silver(I) from aqueous solutions by chitosan/bamboo charcoal composite beads. *J. Clean. Prod.* **87**, 850–855.
Nowruzi, R., Heydari, M. & Javanbakht, V. 2020 Synthesis of a chitosan/polyvinyl alcohol/activate carbon biocomposite for removal of hexavalent chromium from aqueous solution. *Int. J. Biol. Macromol.* **147**, 209–216.
Phillip, W. A., Yong, J. S. & Elimelech, M. 2010 Reverse draw solute permeation in forward osmosis: modeling and experiments. *Environ. Sci. Technol.* **44**, 5170–5176.
Qasim, M., Darwish, N. A., Sarp, S. & Hilal, N. 2015 Water desalination by forward (direct) osmosis phenomenon: a comprehensive review. *Desalination* **374**, 47–69.
Qasim, M., Mohammed, F., Aidan, A. & Darwish, N. A. 2017 Forward osmosis desalination using ferric sulfate draw solute. *Desalination* **423**, 12–20.
Qi, S., Qiu, C. Q., Zhao, Y. & Tang, C. Y. 2012 Double-skinned forward osmosis membranes based on layer-by-layer assembly – FO performance and fouling behaviour. *J. Membr. Sci.* **405–406**, 20–29.
Queiroz, M. F., Melo, K. R. T., Sabry, D. A., Sassaki, G. L. & Rocha, H. A. O. 2015 Does the use of chitosan contribute to oxalate kidney stone formation? *Mar. Drugs* **13**, 141–158.
Rana, D. & Matsuura, T. 2010 Surface modifications for antifouling membranes. *Chem. Rev.* **110**, 2448–2471.
Ren, J. & McCutcheon, J. R. 2014 A new commercial thin film composite membrane for forward osmosis. *Desalination* **343**, 187–193.
Sairam, M., Sereewatthanawut, E., Li, K., Bismarck, A. & Livingston, A. G. 2011 Method for the preparation of cellulose acetate flat sheet composite membranes for forward osmosis–desalination using $MgSO_4$ draw solution. *Desalination* **273**, 299–307.
Saren, Q., Qiu, C. Q. & Tang, C. Y. 2011 Synthesis and characterization of novel forward osmosis membranes based on layer-by-layer assembly. *Environ. Sci. Technol.* **45**, 5201–5208.
Shaffer, D. L., Werber, J. R., Jaramillo, H., Lin, S. & Elimelech, M. 2015 Forward osmosis: where are we now? *Desalination* **356**, 271–284.
Shakeri, A., Salehi, H. & Rastgar, M. 2017 Chitosan-based thin active layer membrane for forward osmosis desalination. *Carbohydr. Polym.* **174**, 658–668.

Shanmugam, A., Kathiresan, K. & Nayak, L. 2016 Preparation, characterization and antibacterial activity of chitosan and phosphorylated chitosan from cuttlebone of *Sepia kobiensis* (Hoyle, 1885). *Appl. Biotechnol., Rep.* **9**, 25–30.

Sharma, U., Shalini, S., Basu, S., Saravanan, P. & Jang, M. 2021 Active layer modification of commercial nanofiltration membrane using CuBTC/PVA matrix for improved surface and separation characteristics. *J. Appl. Polym. Sci.* **138**, 50508.

Shu, J., Cheng, S., Xia, H., Zhang, L., Peng, J., Li, C. & Zhang, S. 2017 Copper loaded on activated carbon as an efficient adsorbent for removal of methylene blue. *RSC Adv.* **7**, 14395–14405.

Singh, N., Petrinic, I., Hélix-Nielsen, C., Basu, S. & Balakrishnan, M. 2019a Influence of forward osmosis (FO) membrane properties on dewatering of molasses distillery wastewater. *J. Water Process Eng.* **32**, 100921.

Singh, N., Dhiman, S., Basu, S., Balakrishnan, M., Petrinic, I. & Helix-Nielsen, C. 2019b Dewatering of sewage for nutrients and water recovery by forward osmosis (FO) using divalent draw solution. *J. Water Process Eng.* **31**, 100853.

Sun, Y., Xue, L., Zhang, Y., Zhao, X., Huang, Y. & Du, X. 2014 High flux polyamide thin-film composite forward osmosis membranes prepared from porous substrates made of polysulfone and polyethersulfone blends. *Desalination* **336**, 72–79.

Suwaileh, W., Pathak, N., Shon, H. & Hilal, N. 2020 Forward osmosis membranes and processes: a comprehensive review of research trends and future outlook. *Desalination* **485**, 114455.

Tang, C., Zhang, Q., Wang, K., Fu, Q. & Zhang, C. 2009 Water transport behavior of chitosan porous membranes containing multi-walled carbon nanotubes (MWNTs). *J. Membr. Sci.* **337**, 240–247.

Tang, C. Y., She, Q., Lay, W. C. L., Wang, R. & Fane, A. G. 2010 Coupled effects of internal concentration polarization and fouling on flux behavior of forward osmosis membranes during humic acid filtration. *J. Membr. Sci.* **354**, 123–133.

Wang, X., Wang, X., Xiao, P., Li, J., Tian, E., Zhao, Y. & Ren, Y. 2016 High water permeable free-standing cellulose triacetate/graphene oxide membrane with enhanced antibiofouling and mechanical properties for forward osmosis. *Colloids Surf. A Physicochem. Eng. Asp.* **508**, 327–335.

Wang, Y. N., Goh, K., Li, X., Setiawan, L. & Wang, R. 2018 Membranes and processes for forward osmosis-based desalination: recent advances and future prospects. *Desalination* **434**, 81–99.

Wang, X., Ba, X., Cui, N., Ma, Z., Wang, L., Wang, Z. & Gao, X. 2019 Preparation, characterization, and desalination performance study of cellulose acetate membranes with MIL-53(Fe) additive. *J. Membr. Sci.* **590**, 117057.

Wei, J., Qiu, C., Tang, C. Y., Wang, R. & Fane, A. G. 2011 Synthesis and characterization of flat-sheet thin film composite forward osmosis membranes. *J. Membr. Sci.* **372**, 292–302.

Wu, Q. Y., Xing, X.-Y., Yu, Y., Gu, L. & Xu, Z.-K. 2018 Novel thin film composite membranes supported by cellulose triacetate porous substrates for high-performance forward osmosis. *Polymer* **153**, 150–160.

Xiao, T., Nghiem, L. D., Song, J., Bao, R., Li, X. & He, T. 2017 Phenol rejection by cellulose triacetate and thin film composite forward osmosis membranes. *Sep. Purif. Technol.* **186**, 45–54.

Yu, Q., Gutierrez, M. T. G. & Hägg, M.-B. 2018 Using an osmotic membrane pressure actuator (OMPA) for enhanced oil and gas recovery – the concept. *J. Petrol. Sci. Eng.* **3** (2), 48–56.

Zamani, F., Chew, J. W., Akhondi, E., Krantz, W. B. & Fane, A. G. 2015 Unsteady-state shear strategies to enhance mass-transfer for the implementation of ultrapermeable membranes in reverse osmosis: a review. *Desalination* **356**, 328–348.

Zhang, S., Wang, K. Y., Chung, T. S., Chen, H., Jean, Y. C. & Amy, G. 2010 Well-constructed cellulose acetate membranes for forward osmosis: minimized internal concentration polarization with an ultra-thin selective layer. *J. Membr. Sci.* **360**, 522–535.

Zhang, S., Wang, K. Y., Chung, T. S., Jean, Y. C. & Chen, H. 2011 Molecular design of the cellulose ester-based forward osmosis membranes for desalination. *Chem. Eng. Sci.* **66**, 2008–2018.

Zirehpour, A., Rahimpour, A., Seyedpour, F. & Jahanshahi, M. 2015 Developing new CTA/CA-based membrane containing hydrophilic nanoparticles to enhance the forward osmosis desalination. *Desalination* **371**, 46–57.

First received 9 March 2021; accepted in revised form 5 August 2021. Available online 17 August 2021